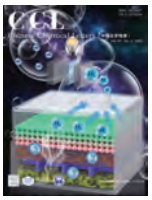
Chinese Chemical Letters 37 (2026) 110825

Contents lists available at ScienceDirect

Chinese Chemical Letters

journal homepage: www.elsevier.com/locate/cclet



Assembly of π-conjugated $[B_3O_7]$ groups by unprecedented antiparallel triangles $[ZnO_3]$ to tailor a deep-UV zinc borate birefringent crystal

Ning Yang[a], Huijian Zhao[a], Wenli Zhao[a], Yuheng She[a], Ning Ye[a], Zhanggui Hu[a], Conggang Li[a,b,*]

[a] Tianjin Key Laboratory of Functional Crystal Materials, Institute of Functional Crystals, Materials Science and Engineering, Tianjin University of Technology, Tianjin 300384, China
[b] State Key Laboratory of Crystal Materials, Shandong University, Ji'nan 250100, China

ARTICLE INFO

Article history:
Received 27 November 2024
Revised 24 December 2024
Accepted 6 January 2025
Available online 7 January 2025

Keywords:
Zinc borate
Deep ultraviolet
Birefringence
Functional motifs
Light modulation

ABSTRACT

Birefringent crystals have gained increasing attention for versatile optical devices due to their inherent ability to modulate light polarization. However, the rational design of structures that exhibit high birefringence and deep-ultraviolet (DUV) transparency remains a formidable challenge. Here, a novel zinc borate birefringent crystal, $Na_2ZnB_6O_{11}$ (NZBO), was identified by strategically assembling the π-conjugated $[B_3O_7]$ functional units using the unprecedented antiparallel triangles formed by $[ZnO_3]$ motifs. Remarkably, through a tailored motif approach and optimized arrangement, NZBO achieves the largest birefringence (0.094) in the visible wavelength range among the borate-based crystals containing $[B_3O_7]$ units, exceeding that of commercially available birefringent crystal MgF_2 by approximately 8 times (0.012@532 nm). Furthermore, NZBO exhibits a notably short DUV absorption cutoff edge below 190 nm along with a wide band gap of 6.04 eV attributed to the elimination of dangling bonds. The origin of the optical anisotropy attributes of NZBO was elucidated through a combination of theoretical calculations and structural analyses. These findings highlight the good potential of NZBO in the manipulation of polarized light and offer valuable insights for tailoring new birefringent materials in the short-wave UV transparency region.

© 2026 Published by Elsevier B.V. on behalf of Chinese Chemical Society and Institute of Materia Medica, Chinese Academy of Medical Sciences.

The interaction between light and matter lies at the core of versatile technologies and holds significant applications in the optoelectronic fields [1]. The macroscopic properties, including ferroelectricity, magnetism, and both linear and nonlinear optical properties, which are influenced by light-matter interaction, are typically determined by the functional motifs of the materials [2]. Birefringence, as a manifestation of spatially asymmetric light-matter interaction, plays a key role in the manipulation of light polarization, which thus has garnered significant interest owing to its essential applications in laser phase-matching, optical communication, and optical interference filters [3–9]. With the expanding demand for deep ultraviolet (DUV) light sources, the fabrication of DUV polarized light using birefringent materials is of particular interest. Unfortunately, a notable challenge remains in designing DUV birefringent crystals with both a wide band gap and substantial birefringence, as these two indicators typically exhibit an inverse relationship [10–16]. For example, MgF_2, a widely used short-wave birefringent crystal, exhibits exceptional DUV transparency down to 110 nm but has a small birefringence of 0.012 at 532 nm, which limits its extended applications [17]. Consequently, very few commercial birefringent crystals can simultaneously meet the required specifications, highlighting the ongoing challenge in exploring high-performance DUV birefringent materials [18–20].

In general, the birefringence of a crystal is primarily related to its anionic framework built by functional motifs and their unique arrangements. Borates, distinguished by their versatile coordination modes and short UV absorption cutoff edges resulting from intense covalent B-O bonds, have been extensively studied as potential candidates for designing DUV birefringent materials. Some functional basic groups based on B-O bonds have shown promise in achieving large optical anisotropy and sufficient birefringence [21–25]. Notable examples such as $[B_3O_6]$-type crystals α-BaB_2O_4 (0.119@546 nm) and $Ba_2Ca(B_3O_6)_2$ (0.12@532 nm), as well as $[BO_3]$-type $Ca_3(BO_3)_2$ (0.098@546 nm) and $LiBO_2$ (0.168@266 nm) [26–29], have demonstrated large birefringence and short UV cutoff

* Corresponding author.
E-mail address: cgli@email.tjut.edu.cn (C. Li).

https://doi.org/10.1016/j.cclet.2025.110825
1001-8417/© 2026 Published by Elsevier B.V. on behalf of Chinese Chemical Society and Institute of Materia Medica, Chinese Academy of Medical Sciences.

edges. Recent studies have also highlighted the potential of $[BO_2]$ and $[B_2O_5]$ units as functional motifs for fabricating DUV birefringent materials, as exemplified by $Li_2Na_2B_2O_5$ (0.095@532 nm) with $[B_2O_5]$ motifs and $K_5Ba_2(B_{10}O_{17})_2(BO_2)$ (0.062@1064 nm) featuring $[BO_2]$ motifs [30,31]. These mentioned materials exemplify the effectiveness of $[BO_2]$, $[BO_3]$, $[B_2O_5]$, and $[B_3O_6]$ groups as birefringence-active chromophores for enhancing optical anisotropy. Conversely, the use of non-condensed $[B_3O_7]$ building units as birefringence-enhanced motifs has shown limited effectiveness, impeding the generation of notable birefringence. For instance, LiB_3O_5 (LBO), a commercially available nonlinear optical crystal, demonstrates a wide DUV transparency range due to the presence of $[B_3O_7]$ groups [32]. Unfortunately, the perpendicular arrangement characterized by the parallel orientation of $[B_3O_7]$ groups in different directions, results in an undesirable birefringence of 0.04 at 1064 nm for LBO [33]. This observation highlights the recognition of compounds featuring $[B_3O_7]$ structural motifs for their advantageous transmission properties in the short-wave UV range [34]. Nevertheless, it is noteworthy that the non-uniform arrangement characteristics exhibited by distinct $[B_3O_7]$ groups can lead to a relatively diminished optical anisotropy [35–37].

Apart from the distinct functional units, the arrangement orientation of these units within the crystal lattice plays a crucial role in determining optical anisotropy [38]. Various strategies have been implemented to regulate the arrangement of functional units, including the incorporation of d^{10} transition metal cations like Zn^{2+}, Cd^{2+}, and Hg^{2+}, which are widely recognized for their potential to enhance microscopic polarization anisotropy [39–42]. For example, the introduction of Zn^{2+} cations effectively adjusts the arrangement of $[BO_3]$ building units in $CaZn_2(BO_3)_2$ [43]. As a result, these units are orderly stacked along the *c* direction, leading to an impressive enlargement of birefringence, with a value of 0.081 at 546 nm. Similarly, the substitution of Cs^+ cations with Hg^{2+} in the Li_2CsPO_4 compound results in the formation of $[HgPO_4]_\infty$ single layers in the *ab* plane, effectively counteracts the inherent rigidity of $[PO_4]$ structural units. This substitution results in a significant sixfold enhancement in birefringence, elevating the value from ~0.01 in Li_2CsPO_4 to 0.068 at 1064 nm in $LiHgPO_4$ [44]. Compared to the heavy Cd^{2+} and Hg^{2+} cations, Zn^{2+} cations not only offer the structural preservation of diverse coordination modes but also the advantage of the lighter elemental mass for broadening UV transparency [45,46]. Therefore, Zn-O based groups can be regarded as birefringence-active functional units in pursuing innovative short-wave birefringent materials. Building upon these principles, we endeavored to introduce Zn^{2+} into borates containing $[B_3O_7]$ units to optimize the arrangement of functional units and enlarge birefringence. Additionally, the incorporation of Zn-O groups can eliminate the dangling bonds by connecting the terminal O atoms of B-O groups, contributing to a blue shift of UV cutoff edges. Through these efforts, we successfully synthesized a novel zinc borate crystal, namely $Na_2ZnB_6O_{11}$ (NZBO), distinguished by the presence of $[B_3O_7]$ groups and planar triangles $[ZnO_3]$. As expected, the arrangement of $[B_3O_7]$ groups was optimized through the incorporation of $[ZnO_3]$ motifs, yielding significantly smaller dihedral angles (70.85°) between adjacent $[B_3O_7]$ groups in comparison with that observed in LBO. Moreover, the $[ZnO_3]$ units display a unique unparallel arrangement, representing an unprecedented observation in the borates. Such structural characteristics contribute to the enhancement of birefringence in NZBO, reaching to 0.094 in the visible wavelength range. To the best of our knowledge, this represents the largest reported value among zinc borate-based materials containing $[B_3O_7]$ units. Moreover, NZBO features a notably short cutoff edge below 190 nm, further highlighting its great potential as a DUV birefringent material. In this study, we present a comprehensive investigation on its synthesis, structure, and optical characterizations of NZBO. Besides, a combination of theoretical calculations and structural analyses was performed to evaluate the underlying factors contributing to its remarkable birefringence.

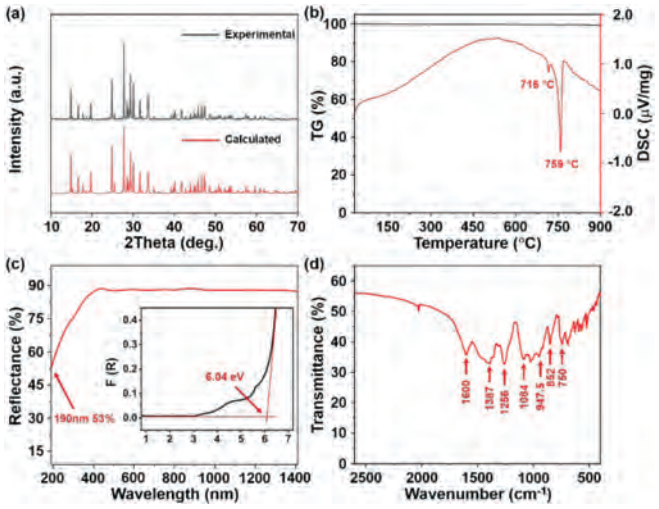


Fig. 1. (a) Matching feature of experimental and calculated PXRD patterns for NZBO. (b) A combination of DSC and TG curves for NZBO. (c, d) Experimental UV–vis-NIR diffuse reflectance spectrum along with band gap and IR spectrum for NZBO, respectively.

Polycrystalline NZBO was experimentally prepared through a high-temperature sintering process. As illustrated in Fig. 1a, the experimental powder X-ray diffraction (PXRD) curves exhibit an excellent match with those derived from the single crystal structure, demonstrating the phase purity of NZBO. As shown in Fig. S1 (Supporting information), further PXRD measurements demonstrates the consistent peak patterns of NZBO before and after melting process. Furthermore, thermal analysis of NZBO reveals two notable endothermic peaks in the DSC curve, located at around 716 and 759 °C, while the corresponding TG curve displays no apparent weight loss (Fig. 1b). It is suggested that there may be a reversible phase transition at about 716 °C. This observation underscores the high thermal stability of NZBO, which extends up to 716 °C. The target crystals were extracted by a spontaneous crystallization approach. As the fact that the process of crystal growth demands continual optimization of growth parameters, including temperature field uniformity and cooling rate, an extensive exploration is needed to achieve bulk crystal growth of NZBO.

UV–vis-NIR diffuse reflectance spectrum shows that the UV absorption cut-off edge of NZBO is below 190 nm, with 53 % absorption at 190 nm (Fig. 1c). The experimental bandgap of NZBO was determined to be 6.04 eV, utilizing the Kubelka-Munk formula. Notably, the UV cutoff of NZBO exhibited a significantly blue-shifted in comparison to other zinc borates like $Zn_3B_2O_6$ (380 nm), $CsZn_2B_3O_7$ (218 nm), and $Zn_4B_6O_{13}$ (217 nm) [47–49]. This is mainly due to the fact that the terminal O atoms of the $[B_3O_7]$ unit are connected by the $[BO_4]$ and $[ZnO_3]$ triangles, which eliminate suspension bonds and shift the UV cutoff edge blue to the DUV region. This favorable transparency positions NZBO as a promising candidate for optical crystals in the short-wave UV range. In addition, we conducted an IR spectrum analysis to characterize the vibrational modes characterized by the building blocks in NZBO. As shown in Fig. 1d, it displays distinctive absorption bands in the range of 1256–1600 cm^{-1}, which can be attributed to the asymmetric stretching vibration of $[BO_3]$ units, while the characteristic peaks located at around 852 cm^{-1} and 1084 cm^{-1} correspond to the stretching-bending vibration of $[BO_4]$ units [50,51]. Additionally, the absorption peaks below 750 cm^{-1} mainly originate from the overlap bending modes of $[BO_3]$ and $[BO_4]$ units

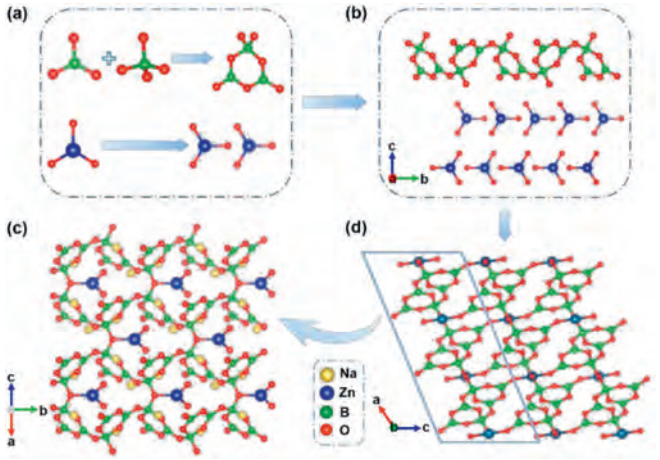


Fig. 2. Structure characterization of NZBO. (a) $[BO_3]$, $[BO_4]$, $[B_3O_7]$ groups, and isolated $[ZnO_3]$ planar triangles. (b) Presentation of the $[B_6O_{13}]_\infty$ chains and antiparallel arrangements of isolated $[ZnO_3]$ units, respectively. (c, d) Presentations of 3D structural network viewed from the *ac* plane and a 90 ° rotation direction, respectively.

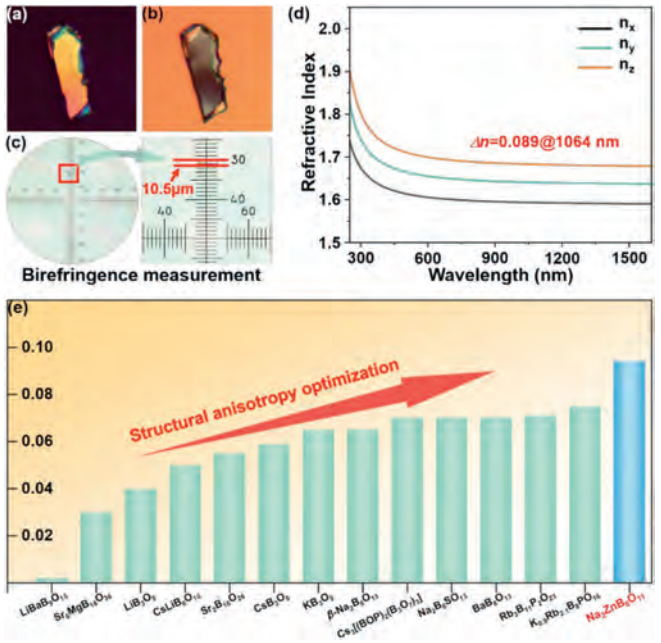


Fig. 3. (a, b) The original interference state and the resulting presentation after extinction of the NZBO crystal under cross-polarized light, respectively. (c) Crystal thickness of NZBO. (d) Calculated refractive index dispersion patterns of NZBO. (e) Comparison of birefringence among the reported short-wave UV transparent borates containing $[B_3O_7]$ groups.

[52,53]. These observed features in the B-O chemical bonds align well with the structural analysis of NZBO.

To elucidate the correlation between performance and structural characteristics, the crystal structure of NZBO was identified through single-crystal X-ray diffraction analysis. The results reveal that NZBO crystallizes in the centrosymmetric monoclinic system with a space group of *C*2/*c* (No. 15), which contrasts with the previously reported structure classified under the acentric space group *Cc* (No. 9) [54]. A detailed comparison of the distinct crystallographic parameters is provided in Tables S1-S3 (Supporting information). The asymmetric unit of NZBO contains three unequal B sites, one unequal Zn site, one unequal Na site and six unequal O sites. As shown in Fig. 2a, the crystallographic independent B atoms exhibit two distinct coordination modes. B atoms are bonded to three and four O atoms, forming distinct $[BO_3]$ triangles and $[BO_4]$ tetrahedra, respectively. The B-O bond lengths for $[BO_3]$ units range from 1.326(4) Å to 1.401(4) Å, with bond angles ranging from 114.1(3)° to 125.4(3)°. For the $[BO_4]$ tetrahedra, the B-O bond lengths range from 1.455(4) Å to 1.509(4) Å, with bond angles ranging from 103.0(3)° to 113.0(3)°. It is observed that two adjacent $[BO_3]$ triangles are connected to a $[BO_4]$ tetrahedron forming the conjugated $[B_3O_7]$ units (Fig. 2a). Remarkably, a rare coordination pattern is observed for Zn atoms, where they exhibit a unique coordination with three O atoms, forming isolated $[ZnO_3]$ planar triangles. The distinct coordination mode of $[ZnO_3]$ unit was just observed in the previously reported zincate compounds $Cs_4(ZnO_3)$ and $Na_{10}Zn_4O_9$ [55,56]. Intriguingly, this geometric configuration represents an unprecedented structural feature in borates, due to the typical tendency of Zn atoms to coordinate with four O atoms to form $[ZnO_4]$ tetrahedra. The Zn-O distances of $[ZnO_3]$ units range from 1.876(2) Å to 1.931(3) Å, with O-Zn-O bond angles spanning from 117.63(16)° to 121.19(8)°. According to previous literature reports, the length range observed in Zn-O bonds of NZBO fall within a reasonable range [57]. As depicted in Fig. 2b, the adjacent conjugated $[B_3O_7]$ building blocks are interconnected *via* corner-sharing oxygen atoms, leading to the formation of one-dimensional (1D) $[B_6O_{13}]$ chains that extend infinitely along the *b*-axis. The presence of such densely packed coordination environments significantly increases the density of $[BO_3]$ units. Notably, the angle between adjacent $[B_3O_7]$ groups in NZBO is significantly smaller compared to the right angle observed in LBO. This optimized arrangement of $[B_3O_7]$ groups in NZBO facilitates the enhancement of polarizability anisotropy. Intriguingly, the isolated $[ZnO_3]$ triangles adopt an antiparallel arrangement in the *bc* plane, which is beneficial for the generation of significant optical anisotropy. Then these infinite 1D chains $[B_6O_{13}]_\infty$ are further interconnected by the $[ZnO_3]$ triangles to build the three-dimensional (3D) structural network of NZBO, as observed in the *ac* plane (Fig. 2c). Fig. 2d showcases the 3D structural configuration rotated 90°, with Na^+ cations occupied the interstitial spaces to ensure charge balance. The results of bond valence calculations (BVS) revealed that the average valence states of Na, Zn, B and O correspond to 1.08, 1.80, 3.05, and 2.02, respectively, closely aligning with their expected oxidation states, which further provides the validity and rationality of the determined structure. EDS analysis was conducted to ascertain the elemental distribution within the NZBO crystal. The results yielded an approximate molar ratio of Na:Zn elements of 2:1 (Fig. S2 in Supporting information), with these components demonstrating a uniform distribution. These observations exhibit a good agreement with the structural analysis of NZBO, further providing the validity and rationality of the determined structure.

The structural analysis of NZBO unveiled a notably structural anisotropy, suggesting the presence of substantial birefringence. To validate this phenomenon, we employed a polarizing microscope to evaluate the birefringence of NZBO. Figs. 3a and b clearly illustrate the different orientations of NZBO crystals before and after complete extinction under orthogonally polarized light. The precise quantification of the NZBO crystal thickness and the optical path difference yielded values of 10.5 μm and 990 nm, respectively (Fig. 3c). Then the experimental birefringence value of NZBO in the visible wavelength range was measured to be 0.094. It is worth noting that although the birefringent behavior exhibited by NZBO is slightly lower than that of the commercialized available birefringent crystal α-BaB_2O_4 (0.116@1064 nm) [58], yet it is approximately 8 times higher than that of the commercialized available short-wave birefringent crystal MgF_2 (0.012@532 nm). Moreover, we performed an assessment of the theoretical birefringence of NZBO (Fig. 3d), yielding a magnitude

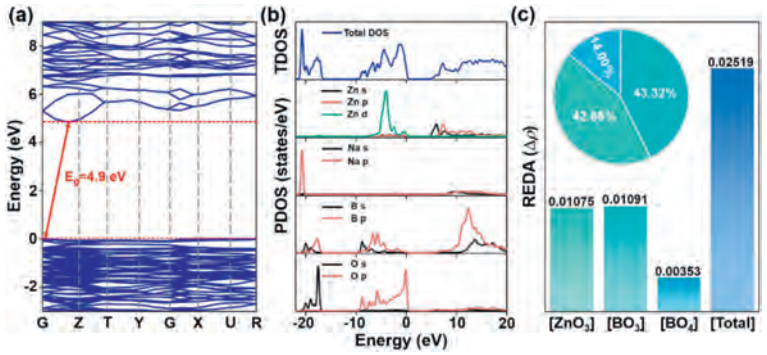


Fig. 4. (a) Band structure for NZBO. (b) PDOS and TDOS for NZBO. (c) The response electron distribution anisotropy analysis of NZBO.

of 0.089 at 1064 nm, which is consistent with the experimental value. To the best of our knowledge, the birefringence value observed in the NZBO crystal is the largest reported value among short-wave UV borate-based materials containing $[B_3O_7]$ units (Fig. 3e and Table S4 in Supporting information). Examples include $LiBaB_9O_{15}$ (0.002@1.06 μm), LiB_3O_5 (0.040@1.06 μm), CsB_3O_5 (0.059@1.06 μm), $CsLiB_6O_{10}$ (0.050@1.06 μm), KB_3O_5 (0.065@1.06 μm), $Cs_3B_{11}P_2O_{23}$ (0.070@1.06 μm), β-$Na_2B_8O_{13}$ (0.065@1.06 μm), BaB_8O_{13} (0.070@1.06 μm), and $K_{0.9}Rb_{2.1}B_8PO_{16}$ (0.071@1.06 μm) [59–65]. The sufficient birefringence and short cut-off edge exhibited by NZBO sheds light on its great potential in the field of light manipulation within the short-wave UV range.

To unveil the underlying origin of optical activities in NZBO, we employed density functional theory (DFT) calculations employing the generalized gradient approximation (GGA). The band structure analysis as shown in Fig. 4a indicated that NZBO can be classified as an indirect bandgap compound, yielding a theoretical band gap value of 4.9 eV, which closely aligns with the experimental value. A further analysis of the total density of states (TDOS) combined with the partial density of states (PDOS) in Fig. 4b demonstrated that the top of the valence bands spanning from around −6 eV to 0 eV are primarily contributed by the Zn 3d and B 2p states, which are hybridized with O 2p states. The bottom of the conduction bands ranging from 5 eV to 10 eV are predominantly composed of the Zn 4s and B 2p states. This analysis indicates that the B-O and Zn-O bond-based groups play a crucial role in its intr–insically optical anisotropy.

To discriminate the influence of different groups on the birefringence properties of NZBO, we further calculated the bonding electron density difference ($\Delta\rho$) of these groups employing the response electron distribution anisotropy (REDA) approach [66]. The observation results revealed that the $[ZnO_3]$, $[BO_3]$ and $[BO_4]$ units contribute approximately 42.68 %, 43.32 % and 14.00 % to the birefringence of NZBO, respectively (Fig. 4c). Indeed, the arrangement of functional primitives in the structural framework emerges as a crucial factor that cannot be overlooked when considering birefringence performance. In the case of $[ZnO_3]$ units, their antiparallel arrangement in the *bc* plane facilitates the superposition of microscopic effects (Fig. 5a), resulting in a significant optical anisotropy in both parallel and perpendicular directions to the layer. Comparable arrangement features and their contributions to birefringence have also been observed in other compounds such as YVO_4 and $Cs_3Nb_5GeO_{16}$ [67]. Furthermore, it is worth noting that the introduction of $[ZnO_3]$ units in NZBO optimizes the arrangement of $[B_3O_7]$ groups. In the 3D B-O framework of LBO, as shown in Figs. 5b and c, adjacent $[B_3O_7]$ groups are vertically arranged, leading to weak optical anisotropy. Conversely, in NZBO, the angle between neighbouring $[B_3O_7]$ groups is reduced to 70.85° (Figs. 5d and e), consequently contributing to the structural anisotropy.

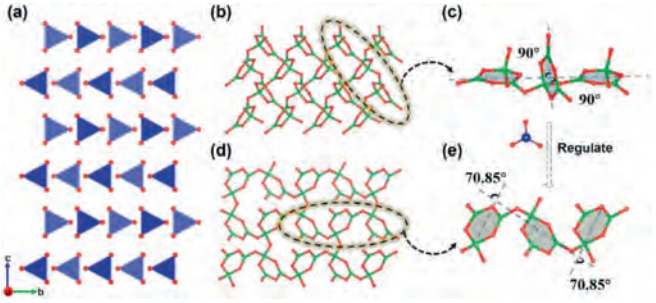


Fig. 5. (a) The isolated $[ZnO_3]$ units are arranged antiparallel in the *c* direction on the *bc* plane. (b, c) B-O bond base structural framework and the arrangement of $[B_3O_7]$ units observed in LBO. (d, e) B-O bond based structural framework and the arrangement of $[B_3O_7]$ units observed in NZBO.

This unique structural arrangement of $[B_3O_7]$ groups in NZBO results in enhanced birefringence compared to that observed in LBO. These findings suggest that the birefringence of NZBO is dominated by the conjugated planar $[B_3O_7]$ and $[ZnO_3]$ units, thus providing valuable insights for further exploration of DUV optical materials characterized by significant birefringence.

In summary, we have successfully identified a zinc borate birefringent crystal, NZBO, through the assembly of the π-conjugated $[B_3O_7]$ functional units and isolated planar triangles $[ZnO_3]$. Notably, the introduction of $[ZnO_3]$ units in NZBO optimizes the arrangement of distinct $[B_3O_7]$ groups, enabling it to exhibit a significant birefringence of 0.094 in the visible wavelength region. To the best of our knowledge, this birefringence value is the largest reported value among the short-wave UV borate-based materials containing $[B_3O_7]$ units. Moreover, this compound possesses a remarkably short UV cutoff edge below 190 nm, indicative of a large band gap of 6.04 eV. Consequently, NZBO achieved a rare combination of large birefringence and wide UV transparency, making it an attractive candidate for short-wave UV birefringent crystals. Additionally, a combination of structural analyses and theoretical calculations suggested that the conjugated planar $[B_3O_7]$ groups and antiparallel $[ZnO_3]$ triangles significantly contribute to the optical anisotropy observed in NZBO. These findings expand the structural chemistry of zinc borates and provide valuable insights for the design of new birefringent materials with high performance.

Declaration of competing interest

The authors declare that they have no known competing financial interests or personal relationships that could have appeared to influence the work reported in this paper.

CRediT authorship contribution statement

Ning Yang: Writing – original draft. **Huijian Zhao:** Writing – review & editing. **Wenli Zhao:** Writing – review & editing. **Yuheng She:** Writing – review & editing. **Ning Ye:** Writing – review & editing. **Zhanggui Hu:** Writing – review & editing. **Conggang Li:** Writing – review & editing.

Acknowledgments

This work was supported by the National Key R&D Program of China (No. 2021YFA0717800), National Natural Science Foundation of China (Nos. 62475191, 61835014), State Key Laboratory of Crystal Materials, Shandong University (No. KF2303).

Supplementary materials

Supplementary material associated with this article can be found, in the online version, at doi:10.1016/j.cclet.2025.110825.

References

[1] F. Naccarato, F. Ricci, J. Suntivich, et al., Phys. Rev. Mater. 3 (2019) 044602.
[2] X. Jiang, S. Deng, M. Whangbo, et al., Natl. Sci. Rev. 9 (2022) nwac017.
[3] H. Chen, M. Ran, S. Zhou, et al., Chin. Chem. Lett. 34 (2023) 107838.
[4] J. Fan, Z. Yan, Z. Chen, et al., Sci. China Chem. 67 (2024) 1–6.
[5] M. Gao, H. Wu, H. Yu, et al., Sci. China Chem. 64 (2021) 1184 –119.
[6] Q. Zhang, R. An, Z. Yang, et al., Sci. China Chem. 67 (2024) 2155–2170.
[7] M. Luo, X. Li, X. Jiang, et al., Chin. Chem. Lett. 35 (2024) 109108.
[8] H. Pei, X. Wang, J. Zhang, et al., Sci. China Chem. 66 (2023) 1073–1077.
[9] L. Wang, C. Tu, H. Gao, et al., Sci. China Chem. 66 (2023) 1086–1093.
[10] G. Shi, Y. Wang, F. Zhang, et al., J. Am. Chem. Soc. 139 (2017) 10645–10648.
[11] T. Tran, H. Yu, J. Rondinelli, et al., Chem. Mater. 28 (2016) 5238–5258.
[12] P. Kumbhakar, S. Adachi, Z. Hu, et al., Jpn. J. Appl. Phys. 42 (2003) 1255–1258.
[13] L. Kang, Z. Lin, J. Qin, et al., Sci. Rep. 3 (2013) 1366–1371.
[14] P. Becker, Adv. Mater. 10 (1998) 979–992.
[15] J. Yu, L. Liu, N. Zhai, et al., J. Cryst. Growth 341 (2012) 61–65.
[16] S. Li, W. Li, X. Li, et al., Chem. Sci. 15 (2024) 8959–8965.
[17] M. Dodge, Appl. Opt. 23 (1984) 1980–1985.
[18] L. Gao, Y. Han, C. Lin, et al., Chin. Chem. Lett. 35 (2024) 109529.
[19] Y. Li, X. Chen, K. Ok, Chem. Commun. 58 (2022) 8770–8773.
[20] A. Tudi, S. Han, Z. Yang, et al., Coord. Chem. Rev. 459 (2022) 214380.
[21] J. Song, X. Kong, C. Li, et al., Inorg. Chem. 63 (2024) 14786–14793.
[22] J. Tan, H. Luo, S. Wang, et al., J. Mater. Chem. C 12 (2024) 13230–13235.
[23] J. Song, H. Zhao, C. Li, et al., Chem. Sci. 15 (2024) 16196–16204.
[24] Y. Zhang, F. Li, R. Yang, et al., Sci. China Chem. 65 (2022) 719–725.
[25] T. Ouyang, X. Chen, S. Chen, et al., New. J. Chem. 48 (2024) 15281–15286.
[26] G. Zhou, J. Xu, X. Chen, et al., J. Cryst. Growth 191 (1998) 517–519.
[27] Z. Jia, N. Zhang, Y. Ma, et al., Cryst. Growth. Des. 17 (2017) 558–562.
[28] S. Zhang, X. Wu, Y. Song, et al., J. Cryst. Growth 252 (2003) 246–250.
[29] L. Lei, D. He, K. He, et al., J. Solid. State. Chem. 182 (2009) 3041–3048.
[30] M. Zhang, D. An, C. Hu, et al., J. Am. Chem. Soc. 141 (2019) 3258–3264.
[31] C. Huang, M. Mutailipu, F. Zhang, et al., Nat. Commun. 12 (2021) 2597.
[32] C. Chen, Y. Wu, A. Jiang, et al., Opt. Soc. Am. B 6 (1989) 616–621.
[33] Y. Zhou, Z. Guo, H. Gu, et al., Nat. Photon. 18 (2024) 922–927.
[34] Q. Wang, F. Yang, X. Wang, et al., Inorg. Chem. 58 (2019) 5949–5955.
[35] H. Liu, H. Wu, Z. Hu, et al., ACS Mater. Lett. 5 (2023) 155–161.
[36] Y. Zhao, L. Zhu, Y. Li, et al., Mater. Chem. Front. 7 (2023) 3986–3993.
[37] Y. Shen, S. Zhao, J. Luo, Coord. Chem. Rev. 366 (2018) 1–28.
[38] Y. Zheng, Z. Wei, H. Wu, et al., Mater. Today Phys. 46 (2024) 101529.
[39] Y. Zhou, X. Zhang, M. Hong, et al., Sci. Bull. 67 (2022) 2276–2279.
[40] J. Zhou, P. Gong, M. Xia, et al., Inorg. Chem. 62 (2023) 8931–8939.
[41] C. Zhao, D. Lu, X. Tian, et al., Inorg. Chem. 62 (2023) 21487–21496.
[42] H. Yu, H. Wu, S. Pan, et al., J. Am. Chem. Soc. 136 (2014) 1264–1267.
[43] M. Mutailipu, F. Li, C. Jin, et al., Angew. Chem. Int. Ed. 61 (2022) e202202096.
[44] B. Wu, C. Hu, F. Mao, et al., J. Am. Chem. Soc. 141 (2019) 10188–10192.
[45] Z. Fang, C. Hu, W. Chen, et al., Inorg. Chem. Front. 9 (2022) 5188–5194.
[46] S. Shu, J. Huang, C. Hu, et al., Chem. Eur. J. 28 (2022) e202103401.
[47] S. Wang, X. Zhang, Adv. Mater. 31 (2019) 1805432.
[48] S. Zhao, J. Zhang, S. Zhang, et al., Inorg. Chem. 53 (2014) 2521–2527.
[49] X. Jiang, M. Molokeev, P. Gong, et al., Adv. Mater. 28 (2016) 7936–7940.
[50] N. Ye, W. Zeng, B. Wu, et al., Proc, SPIE 3556 (1998) 21–23.
[51] J. Sun, M. Mutailipu, S. Pan, et al., Chem. Eur. J. 27 (2021) 8698–8703.
[52] G. Peng, N. Ye, Z. Lin, et al., Angew. Chem. Int. Ed. 57 (2018) 8968–8972.
[53] M. Luo, F. Liang, Y. Song, et al., J. Am. Chem. Soc. 140 (2018) 3884–3887.
[54] Y. Chen, J. Liang, Y. Gu, et al., Powder. Diffr. 25 (2010) 9–14.
[55] M.J. D.Trinschek, Z. Anorg, Allg. Chem. 622 (1996) 245–250.
[56] C. Hoch, Z. Naturforsch. 66b (2011) 1248–1254.
[57] Y. Chen, M. Zhang, M. Mutailipu, et al., Molecules 24 (2019) 2763.
[58] Z. Chen, H. Zeng, S. Han, et al., Inorg. Chem. Front. 8 (2021) 2584–2590.
[59] H. Zheng, Y. Li, X. Zhang, et al., Inorg. Chem. Front. 9 (2022) 5360–5370.
[60] C. Chen, Z. Lin, Z. Wang, Appl. Phys. B 80 (2005) 1–25.
[61] R. Bubnova, V. Fundamenskii, S. Filatov, et al., Dokl. Phys. Chem. 39 (2004) 249–253.
[62] H. Liu, H. Wu, Z. Hu, et al., J. Am. Chem. Soc. 145 (2023) 12691–12700.
[63] N. Penin, M. Touboul, G. Nowogrocki, J. Solid. State. Chem. 168 (2002) 316–321.
[64] S. Volkov, V. Yukhno, R. Bubnova, et al., Cryst. Growth. Des. 22 (2022) 6267–6274.
[65] W. He, X. Zhu, Z. Hu, et al., Inorg. Chem. 63 (2024) 19023–19029.
[66] B. Lei, Z. Yang, S. Pan, Chem. Commun. 53 (2017) 2818–2821.
[67] W. Zhao, J. Jiao, Y. She, et al., Adv. Opt. Mater. 10 (2022) 2201704.